RSC Advances

ROYAL SOCIETY OF CHEMISTRY

www.rsc.org/advances

Cite this: DOI: 10.1039/c0xx00000x

www.rsc.org/xxxxxx

ARTICLE TYPE

Dose Dependent Distribution and Aggregation of Gold Nanoparticles within Human Lung Adeno-carcinoma Cells

Sheng-Hann Wang,‡[a,b] Chia-Wei Lee,‡[b] Kun-Ching Shen,[b] Fan-Gang Tseng,[a,b] and Pei-Kuen Wei*[b,c]

Received (in XXX, XXX) Xth XXXXXXXXX 20XX, Accepted Xth XXXXXXXXX 20XX

DOI: 10.1039/b000000x

In this work, we discussed the distribution, aggregation and cytotoxicity of different treated doses, 0.01, 0.05, 0.1, 0.2 and 0.5 nM, of poly (allylamine hydrochloride) (PAH) coated gold nanoparticles (Au NPs) with human lung adeno-carcinoma cell line - A549 cells. By taking colorful scattering images and employing the chromatic analysis, the evolution of Au NPs during cellular endocytosis and their distribution were revealed. With the less treated doses, 0.01 and 0.05 nM, Au NPs were mostly endocytosed and then clustered as larger aggregates inside cells. When treated dose was increased to 0.1 or 0.2 nM, a number of Au NPs were stuck on the membrane and formed two scattering color bands, yellow for larger aggregates inside cells and green for individual NPs on the membrane. By comparing with the cells treated with 0.1 nM Au NPs and dynasore, we can find the PAH coated Au NPs were up-taken into cells *via* the dynamin dependent endocytosis. For the 0.5 nM, different from the 0.1 and 0.2 nM, there are large numbers of Au NPs stuck on the membrane, and furthermore, owing to the periodic lamellipodial contraction with rearward actin polymerization on the membrane, stuck Au NPs were moved to and accumulated on the top of cells. From scanning electron microscopy (SEM) images, we find that the number and density of Au NPs stuck on the membrane was increasing with the increasing treated dose. Dual-beam focus ion beam (DBFIB) images showed the 2D covering and 3D stacking of the aggregated Au NPs on membrane and inside endocytic vesicles respectively. Cytotoxicity test indicates the stuck Au NPs on the membrane would efficiently impact the cell viability. This work highlights the importance of an overall distribution of Au NPs in the NPs-cell interacted system.

Introduction

Over past decades, gold nanoparticles (Au NPs) have been widely used in biomedical application as either the contrast agents or drug/gene carriers.[1-5] All these applications are based on the interactions of Au NPs and cells, for example, adhering, endocytosis, even penetrating. Previous studies suggest that the differences in uptake and distribution are dependent on the characters of Au NPs, such as size and surface modification.[6-8] Furthermore, these different interactions would further change cellular proliferation, regulation and so on.[9] It also indicates that Au NPs for specialized uses can be thus designed. However, despite the rapid progress and early acceptance of Au NPs in biomedical trials,[10, 11] concerns about their potential toxicity is also arising. Compared to other nanoparticle system, such as quantum dots (CdSe/ZnS) and carbon nanoparticles, Au NPs show the better biocompatibility than the others.[12-14] However, investigations also brought forth notable data regarding the cytotoxicity of Au NPs dependent on the size, surface modification and, especially the exposed dose.[15-17] Of the treatment of Au NPs with cells, too little dose could not achieve the expected result, while within the over treating, side effect would be caused. For example, T. Mironava et al. found that with an increasing concentration of treated Au NPs, cells show a notable increasing percentage in apoptosis.[18] J. Davda et al. pointed out the over treating would reduced the efficiency of NPs that enter cells.[19]

Aside from the treated dose, recent literatures also point out that the distribution of different types of Au NPs hugely impacts their cytotoxicity.[20-22] For instance, Au NPs inside cells by the endocytosis have been demonstrated that they would finally accumulated in lysosomes,[23] and the toxicity is mainly caused by the release of the toxic ion - $Au^{1+/3+}$ in the acid environment. In comparison, no obvious toxicity was caused from the Au NPs which scatter in cytosol. Furthermore, aggregations of NPs and their distribution in biological system might result in different consequence. For example, in the system of the NPs-based drug/gene delivery, if the aggregation of NPs occurred before being endocytosed, it might reduce the uptake of NPs which reduce the efficiency and increase their cytotoxicity.[24, 25] On the other side, if the aggregation occurred after endocytosis, i.e. in the endosome, it might facilitate the release of the NPs from the endosome and increase the efficiency.[26] Therefore, a thorough understanding of the distribution and aggregation of Au NPs and their consequent cytotoxicity would be a key issue for their biomedical applications.

In this work, we study the distribution, aggregation and cytotoxicity of Au NPs with different treated concentration (0, 0.01, 0.05, 0.1, 0.2 and 0.5 nM). Au NPs with 50 nm in diameter and human lung adeno-carcinoma cells A549 were used here. Thanks to the strong scattering property of Au NPs, the clusters of Au NPs can be clearly observed under the dark field illumination. Furthermore, owing to the local surface plasmon resonance (LSPR) coupling effect of Au NPs,[27] the number of Au NPs and their clusters in cells could be estimated by using the chromatic analysis as reported in our previous effort.[28] Sectional dark field microscopy,[1] scanning electron microscopy (SEM, FEI Nova 200) and dual-beam focus ion beam (DBFIB, FEI Helios 600) were used to verify the distribution of Au NPs with cells. To understand the difference in the cellular uptake processes of Au NPs with different treated concentration, the trails of the adhesion and following evolution were also observed under a dark field illumination. Cell viability with different treated concentration of Au NPs was also determined using the MTT assay. The relation between the distribution, aggregation and cytotoxicity of Au NPs with different treated concentration was then compared. This work highlights the significant consequences of different dose treating of Au NPs. As either drug/gene carrier or contrast agent, the dose-optimization of the efficacy and safety of NPs are stressed in nanomedicine and nanotoxicology. By inspecting the distribution, aggregation and their caused cytotoxicity, it helps us to think over the use of NPs, as well as improve or redesign the function of the used NPs in the nanomedicine.

Experimental section

Materials

Gold nanospheres with 50 nm in diameter were obtained from Nanopartz with original particle concentrations of approximately 5.38×10^{10} particles per milliliter. Poly (allylamine hydrochloride) (PAH, Mw~15,000), dynasore, glutaraldehyde and dimethyl sulfoxide (DMSO) were obtained from Sigma-Aldrich. F-12K cell culture medium, fetal bovine serum (FBS), antibiotic penicillin streptomycin amphotericin (PSA) were from Gibco, Invitrogen. 99.99% ethanol was purchased from Merck, Taiwan.

Cell culture

A549 adeno-carcinoma cells were cultured in the F-12K contained 10% FBS and 1% PSA. Cells were incubated in a 37 ℃ and 5 % CO_2 incubator. In the experiment, the cells (10^6 cells per mL) were implanted into the microchip with a cell-cultured cavity (1 cm × 3 cm × 120 μm) for overnight.

Setup

The setup was based on the Olympus upright microscopy BX41. 100x (N.A.＝0.6~1.3) oil type objective lenses was used in the sectional dark field microscopy. 40x air type (N.A.=0.6) was used in the experiment of dynamic trail. Different to 40x air type objective, the 100x oil objective lens was mounted on a PZT stage controlled by a function generator. A zig-zag voltage ramp was generated to have a scanning along the Z axis for the axial section. Once the CCD was activated, the shutter would be opened and then a 20W metal halide light was obliquely incident into the sample by the Cyto Viva setup, and the frame grabber began the synchronic images sequence recording. Cells were implanted inside a homemade microfluidic chip which was configured by acrylic junctions, glass and double-sided tapes as shown as shown in Fig. S1. During the experiment, fresh medium were kept flow into the chamber at a rate of 1 μL min^{-1} by the syringe pump to keep a fluidic environment. At the beginning of the experiment, Au NPs (100 μL with different concentration, 0.01, 0.05, 0.1, 0.2 and 0.5 nM) would be injected into the chip. Microscopy, chip contained cells and syringe pump with medium were placed inside an incubator at 37℃ and 5% CO_2 atmosphere as shown in Fig. S1.

Chromatic analysis of Au NPs clusters

The analysis of aggregated Au NPs is based on our pervious study in ref. [28]. Briefly, the chromatogram of different aggregated number of Au NPs was first established by cross-referencing their scattering image and SEM images. As a result of the coupling of the LSPR in high order mode,[27] the increasing in the aggregated number of Au NPs would induce their scattering color redden, i.e. from green to yellow-orange, and red. Once the relation between the scattering color and their aggregated number was established, we can estimate the number of Au NPs number inside each bright spots (Au NPs clusters) under the dark field illumination even within the cell environment. Scattering images of Au NPs within cells were first transferred from RGB to HSB (hue, saturation and brightness) color space by using a Matlab program. The ratio of the brightness to hue of each Au NPs cluster was then calculated. By applying the chromatogram-aggregated number relation established before, the number of every cluster was calculated. This chromatic analysis method was also validated by inductively coupled plasma mass spectrometry (ICP-MS) as described in ref. [28].

Functionalization of Au NPs

The commercial Au NPs were initially stabilized by citrate anions and possess negative charges on its surface. Compared to the citrate coating, the coating by PAH can increase the attachment to the cells, which is owing to the negative charge of the cellular membrane,[29] and its stabilization in the culture medium. Fig. S2 (a) and (b) shows the cells treated with citrate coated Au NPs. We can find that there are only few Au NPs attached on the cells, while these Au NPs present as large aggregates in the culture medium. Thus, in the following experiments, we modified the surface of Au NPs with PAH to increase its stability and cellular adsorption. PAH coating Au NPs was made by adding 1 wt% PAH into citrate stabilized gold nanospheres solution (900 μL, ~4.5×10^{10} NPs/mL) for two hours (the final PAH concentration was 0.1 wt%). The unbound polymers were then removed and Au NPs (1 mL in microtube) were subsequently washed twice by adding deionized water (DIW) and concentrated with the final concentration 2 nM, ~1.2×10^{11} nps/mL). Au NPs were then added into medium with different concentration (0.01, 0.05, 0.1, 0.2 and 0.5 nM) in concentration and subsequently injected into the microchip for the following experiments. UV-Vis spectra of these Au NPs with different surface modification and concentration were shown in Fig. S3.

Inductively coupled plasma mass spectrometry (ICP-MS) analysis

For the ICP-MS experiments, the cells were cultured in 48 wells culture dish at an initial density of ~10^4 cells per millilitre. After 24 hours, different doses of PAH-coated Au NPs were added to the medium. After 5 minutes, cells were washed with culture medium thrice to remove the unbound NPs. After 8 hours, cells were trypsinized, collected and then sonicated for 10 minutes to disrupt the cell membranes. Au NPs was dissolved by adding 0.3 mL aqua regia. The concentration of gold was determined by ICP-MS(ICP-MS Xseries II, Thermo) and converted to the number of Au NPs per cells.

Specimen preparation for scanning electron microscopy (SEM)

For the inspection for the SEM, cells were first treated with different concentrations of Au NPs, and cultured for 8 hours in the micro-fluidic environment as described in the setup section. Cells were then fixed by 2.5% glutaraldehyde for 2 hours, and dehydrated by using 99.99% ethanol. Samples were following dried by using the critical point dryer (Leica EM CPD300) and subsequently coating with 20 nm gold film by sputter for either EM or DBFIB inspection.

Cytotoxicity evaluation

To evaluate the cytotoxicity of Au NPs with different concentration, the 3-(4,5-dimethylthiazol-2-yl)-2-5-diphenyltetrazolium bromide (MTT) assay was used. The A549 cells were incubated in 96 well plates with a density of 10^4 cells per well overnight at 37℃ and 5% CO_2 atmosphere. Different concentrations of Au NPs were then added into each well. After 5 minutes, the suspended Au NPs were washed away twice by F-12K cell culture medium rinsing. For the endocytosis-inhibited experiment, cells were per-treated with 160 μM dynasore for 1 hour. Plus, the culture medium used in the endocytosis-exhibited experiments before MTT test was always contained 160 μM dynasore. Cell viability was then evaluated using MTT after extra 8 hours' interaction with Au NPs. The medium in each well was first removed and replaced with 100 μL fresh culture medium. 10 μL of 12 mM MTT dissolved in PBS was added into each well. The culture plates were incubated at 37 ℃ and 5% CO_2 atmosphere for 4 hours. After removal all but 50 μL of the medium, 100 μL of DMSO was added to each well and sample was incubated at 37℃ for 10 minutes to dissolve the dye. The absorbance at 540 nm was measured using a microplate reader.

Results and discussion

Scattering images and chromatic analysis

Fig. 1 shows a series of scattering images of cells treated with different concentration of Au NPs at t= 8 hours. Compared to cell, Au NPs clusters show a fantastic color (green and yellow spots) under the dark field illumination. According to previous studies, different color of Au NPs clusters indicates different aggregated number.[28, 30] To quantify the relation between the treated concentration of Au NPs and their cellular uptake, chromatic analysis was employed.[25]. Chromatic analysis can be used to calculate the total number of Au NPs per cell by summing the number of Au NPs in every cluster. Fig. 2(a) shows the calculated total number of Au NPs per cell by using chromatic analysis and ICP-MS. We can find that these two analysis methods show a similar result, thus as the treated concentration was increasing, the total number of Au NPs per cell was also increasing. It indicates the reliability of the chromatic analysis, and this result is in good agreement with the scattering image as shown in Fig. 1. In this work, Au NPs were only treated at the beginning, it can be considered as a "source-limited" case. Compared to the other previous works which were "source-sufficient", i.e. cells were always immersed in the NPs contained medium during the experiment.[24, 31, 32] However, both of these two cases shows similar results. Generally, with the same interaction time, the higher concentration of NPs can stand a higher chance in interaction with cells and following increase the number in uptake.

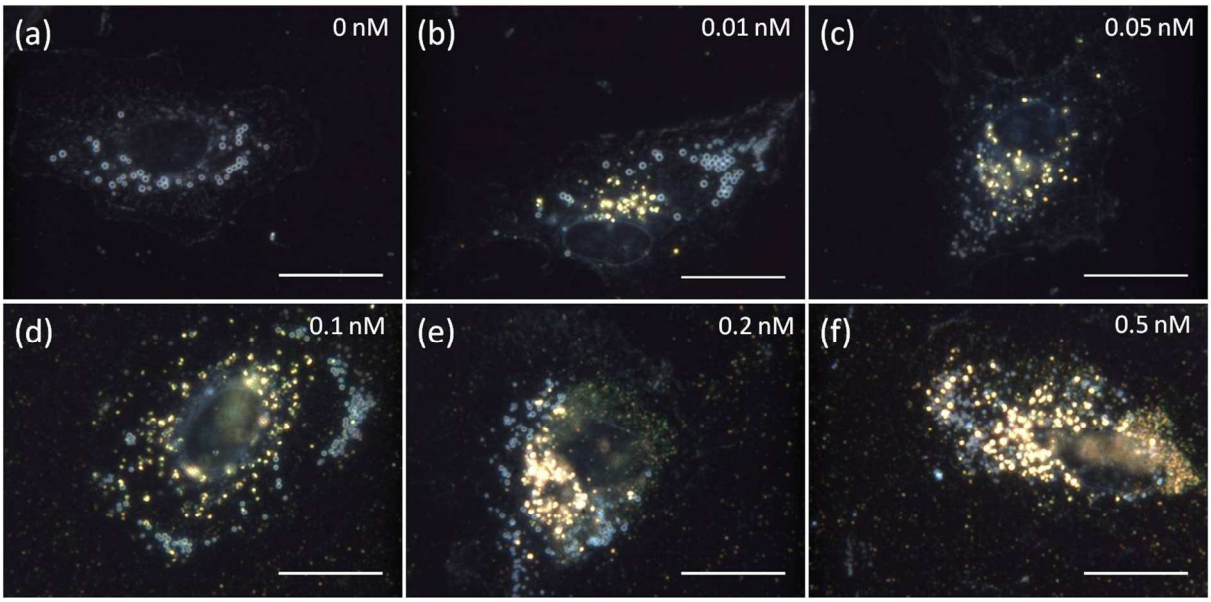

Fig. 1 Scattering images of A549 cells after treated with different concentration Au NPs for 8 hours. Scale bar = 20 μm

Cite this: DOI: 10.1039/c0xx00000x

www.rsc.org/xxxxxx

ARTICLE TYPE

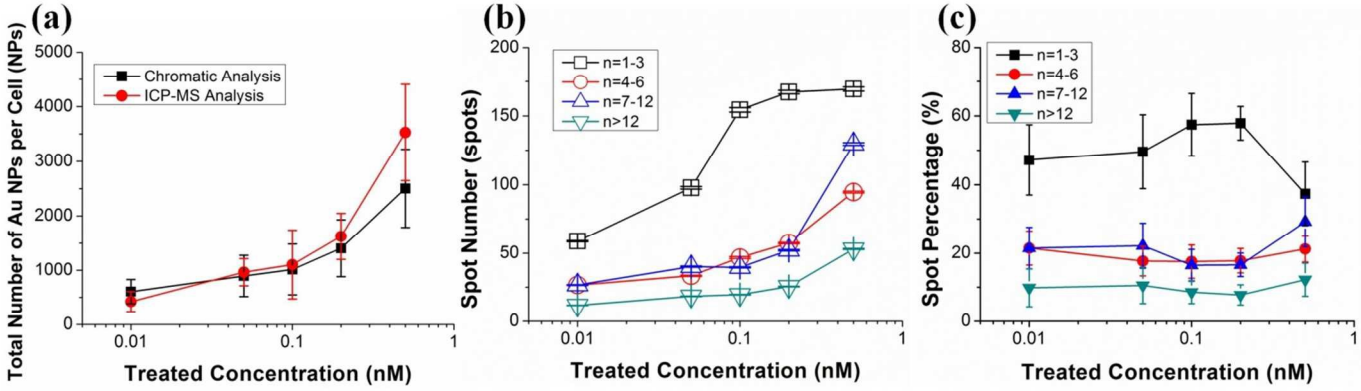

Fig. 2 (a) Total number per cell, (b) spot (cluster) number, and (c) spot (cluster) percentage of Au NPs with different treated concentration per cell. Data represented as standard error of mean in (b), sample number =45.

In our previous study,[33] we found that the PAH coated Au NPs (0.1 nM) were up-taken into cells via dynamin dependent endocytosis, and the color change was due to the progressive sorting by the fusion of the endocytosis in cells. As shown in Fig. S2 (c-d) and Movie 1, Au NPs were firstly scattered on the cell as green dots, and then green dots start decreasing and yellow spots start appearing, it indicates the happening of the aggregation of Au NPs. In comparison, in the case of cells treated with dynasore, an inhibitor of all the dynamin dependent endocytosis,[34, 35] there are no obvious aggregation happening. Again, this result clarified the Au NPs were up-taken into cells via dynamin dependent endocytosis, and different color spots indicate different sizes of Au NPs clusters, or in general, the cargos in cellular vesicle at different endocytic states. Vesicle formation provides a means of cellular entry for extracellular substances. Although ICP-MS is excellent in quantification, it is hard to distinguish the aggregation of Au NPs. In comparison, chromatic analysis can provide additional information in aggregation of Au NPs with cells. In the following experiment, to simplify the vesicle formation, here, we categorized the number of Au NPs in the cluster into four groups. They are the aggregate number n=1~3, 4~6, 7~12 and n>12 respectively. Every group is roughly twice the prior one. The categorization is based on the assumption of the homotypic endocytosis process, that is the endocytic vesicles containing cargos (Au NPs in this work) would undergo either homotypic fusion to form a larger new endosome which carries the combined cargos of the original ones, or homotypic fusion to form two smaller new endosomes each other contain half of the cargos of the original one.[36] Fig. 2(b) shows the spot number of each aggregated group with different treated doses. We can find that with the concentration increasing, the numbers of color spots (Au NPs clusters) of each group were also increasing. However, the increasing rate of each group seems not to be homogeneous. There are abruptly increases within the range from 0.05 to 0.1 nM while reached a plateau in the range from 0.2 to 0.5 nM of n=1~3. For n=7~12, the spot number expands slowly at the concentration less than 0.2 nM, but abruptly increase at 0.5 nM. In comparison, the others show a much stable expansion within the increase of the treated dose.

Fig. 2(c) shows the spot percentage of each aggregated group. From the data, we can further find the abruptly change in n=1~3 and n=7~12 at the treated doses of 0.1 and 0.5 nM. In order to have more deep comprehension of the formation in these different clustering of Au NPs, sectional scattering images and the trail of the Au NPs in cellular uptake were inspected. In the receptor-mediated endocytosis evolution of NPs, mono-dispersed NPs are usually found on or near by the membrane. As the endocytosis progressing, NPs are expected to be sorted and clustered in endo-lysosomes inside the cell.[30, 32, 37] However, in the case of 0.1, 0.2 and 0.5 nM, Au NPs shows some different endocytic behaviour. For the 0.1 and 0.2 nM, there are two kinds of color bands, one is yellow scattered near the nucleus, and the other one is on the membrane which is green (indicates the individual nanoparticles) as indicates in Fig. 3(a) and 3(b). For the 0.5 nM, all the spots show as yellow, while distribute in two different areas as major, beside the nucleus and stack on the membrane as indicates in Fig. 3(c).

Trails of the cellular uptake and following evolution with different treated doses (0.1, 0.2 and 0.5 nM) of Au NPs are shown in Movie 1-3, respectively. In the cases of 0.1 nM and 0.2 nM treatment, green spots, the mono-dispersed Au NPs scattered all over the cells in the beginning. As time goes on, Au NPs started to move toward the center of the cell, and yellow spots, the clustering NPs, was beginning to reveal simultaneously. After a while, the number of green and yellow spots seems to come to a stable state, i.e. no more new clustering of Au NPs achieved. Finally, two different aggregated areas were formed. By inspecting the scattering images that at different focal plane (z=0.96 and z=4.8 μm) as shown in Fig. 3(a) and (b), the locations of the aggregated areas were further revealed. We can find that there are two different areas in major, yellow beside the nucleus that mostly in the bottom of the cells, and green on the

membrane (indicated by the arrowheads in the bottom rows of Fig. 3(a) and (b)). In comparison, in the case of 0.5 nM treatment as Movie 3 shown, although green spots were moved to the center and yellow spots were revealed simultaneously in the beginning as same as in 0.1 and 0.2 nM, there were no green spots remained. As a result, there are still two areas in major, while both of them are yellow spots instead. Fig. 3(c) shows the different focal plane (z=0.96 and z=4.8 μm) of the scattering images in the case of 0.5 nM, and these two aggregated areas were found in different locations; one is beside nucleus in the bottom of the cell, the other is on the membrane as indicated by the arrowhead in the bottom rows of Fig. 3(c). We attributed this difference to the cooperation of the actin polymerization and endocytic processes at the plasmon membrane.[38, 39] As described before, Au NPs were expected to be clustered inside cells and resulted in the change of the scatter color from green to yellow. However, when the number of the treated Au NPs were too large, cells would be very difficult to deal with all of them to the endocytosis from membrane into cells. At the meanwhile, the periodic lamellipodial contraction with actin polymerization is still in work on the membrane, the undealt Au NPs would be thus concentrated to the center, the top of the cell as what we saw in Fig. 4 (a) and 4(b). As the treated dose was still increasing to 0.5 nM, coupling of the LSPR would also be induced by the highly concentrated un-endocytosed Au NPs on the membrane, it means the scatter color would also be changed from green to the yellow.

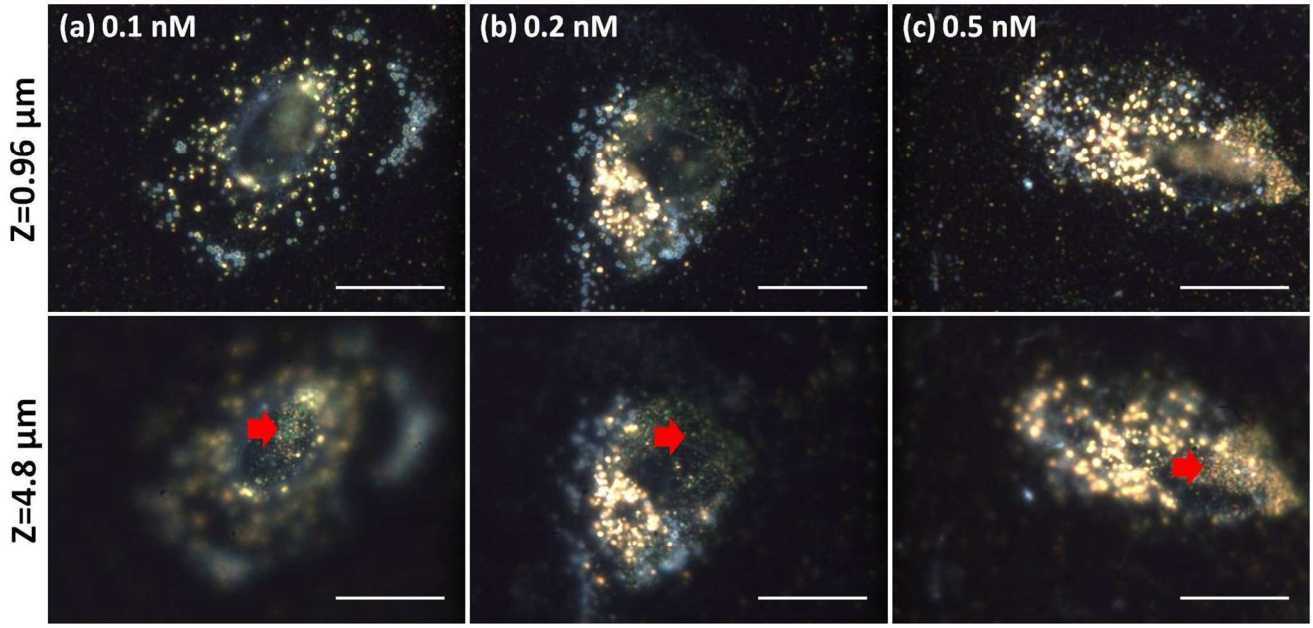

Fig. 3 Sectional scattering images at different focal plane z = 0.96 and 4.8 μm with treated dose (a) 0.1, (b) 0.2 and 0.5 nM. Scale bar = 20 μm.

Cite this: DOI: 10.1039/c0xx00000x

www.rsc.org/xxxxxx

ARTICLE TYPE

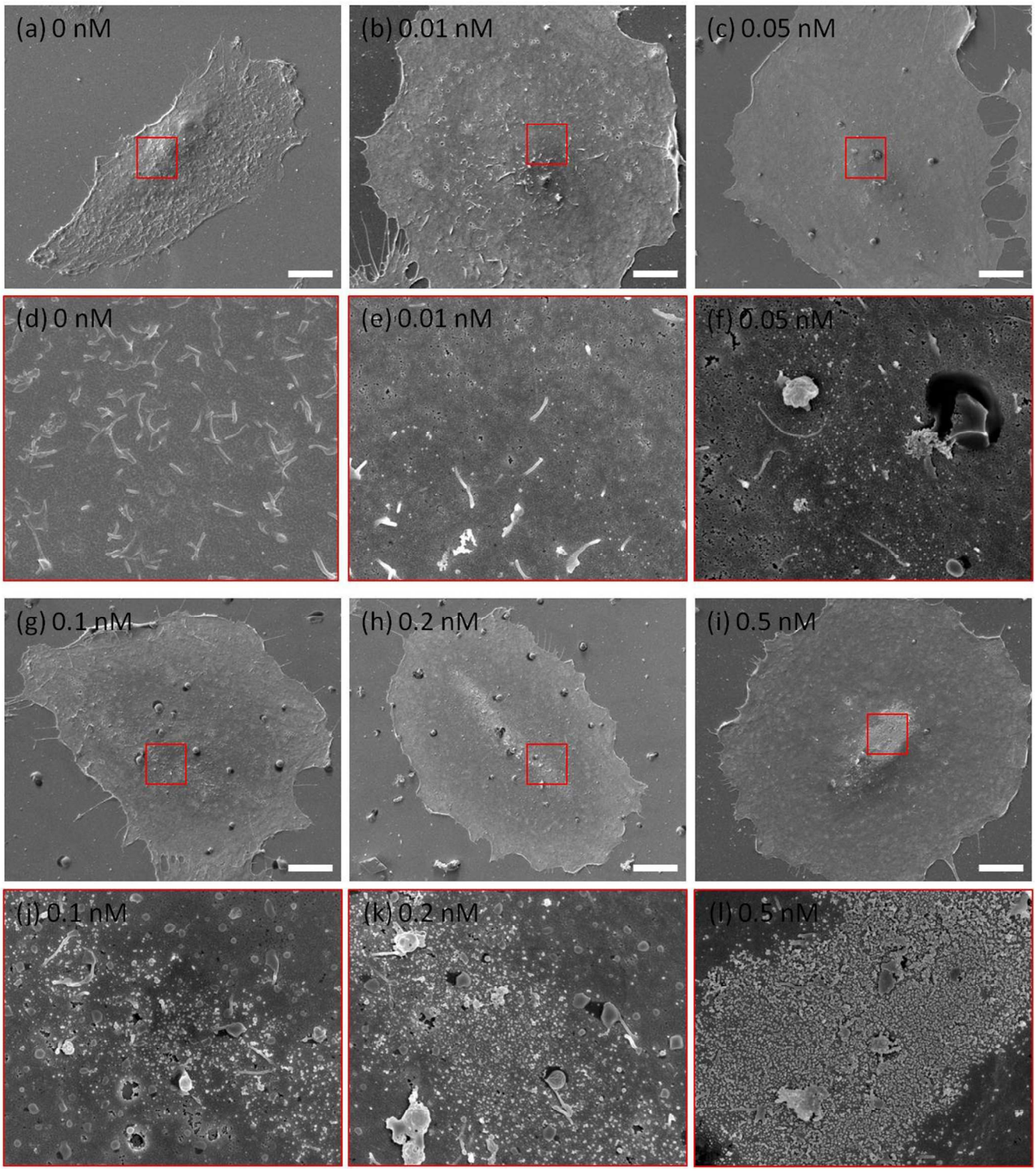

Fig. 4 SEM images of A549 cells with different treated dose of Au NPs. (a-c) Cells treated with 0, 0.01 and 0.05 nM of Au NPs, and (d-f) is the zoom-in of the red frame with the area ~ 10 ×9 μm^2 in (a-c) respectively. (g-h) Cells treated with 0.1, 0.2 and 0.5 nM of Au NPs, and (j-l) shows the zoom-in of the red frame with the area ~ 10 ×9 μm^2 as shown in (g-h) respectively. Note, fibers shown in (d) and (e) are the cilia of A549.Scale bar =10 μm.

Cite this: DOI: 10.1039/c0xx00000x

www.rsc.org/xxxxxx

ARTICLE TYPE

Demonstration of the distribution of Au NPs by SEM and DBFIB

SEM was also used to demonstrate the distribution of Au NPs on the membrane. As shown in Fig. 4, we can easily find the Au NPs aggregates on the top of the cells of the "over treatment" (0.2-0.5 nM), It is noted that even for the "under treatment" (0.01 and 0.05 nM), there are still remained some individual NPs on membrane. It indicates that, in the NPs-cell interactions, especially in the studies of the endocytosis, maybe not all of the NPs would be endocytosed, portion of NPs would be left on the membrane somehow. With the increasing of treated dose, the number and density of the Au NPs on the membrane was also increased. Fig. 5 shows the density of Au NPs in the aggregated bands on the top of cells. The data further verify the different color presented of the aggregated bands in the scattering images of Fig. 3.

DBFIB were then used to determine the difference between the endocytosed and "un-dealt" Au NPs in and on cells respectively. Cases of 0.1 and 0.5 nM were studied. Fig. 6 shows the scattering images and their corresponding SEM images. We can find the "un-dealt" Au NPs were scattered on the membrane as more individual at 0.1 nM treatment. As the treated dose was increased to 0.5 nM, they formed a "2-D quilt" covered on the cell as same as shown in Fig. 4(l). By the DBFIB cutting, Au NPs aggregates in the endocytic vesicle were also revealed. Different from the "2-D quilt" on cells, Au NPs show as 3-D stacks inside both in 0.1 and 0.5 nM (stacks of SEM sectional images are shown in Fig. S4). It indicates that Au NPs can form a larger aggregation inside cells than on the cell membrane. In other words, the concentrated density on the membrane is limited by the 2-D space. The special resolution of this optical system is about 0.25~0.3 μm, and after calculation, there is around 7~12 NPs under the resolution. It also explained why the most increase in spots number is the aggregated number n=7~12 rather than n>12 in Fig.3 (b) and (c), although both of them were increasing at 0.5 nM.

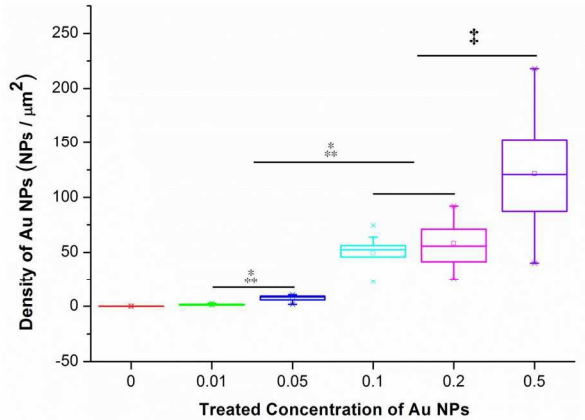

Fig.5 Density of Au NPs on the aggregates band of cells treated with different dose of Au NPs. ‡ p-value < 0.01, ⁂ p-value <0.005. Sample number =15.

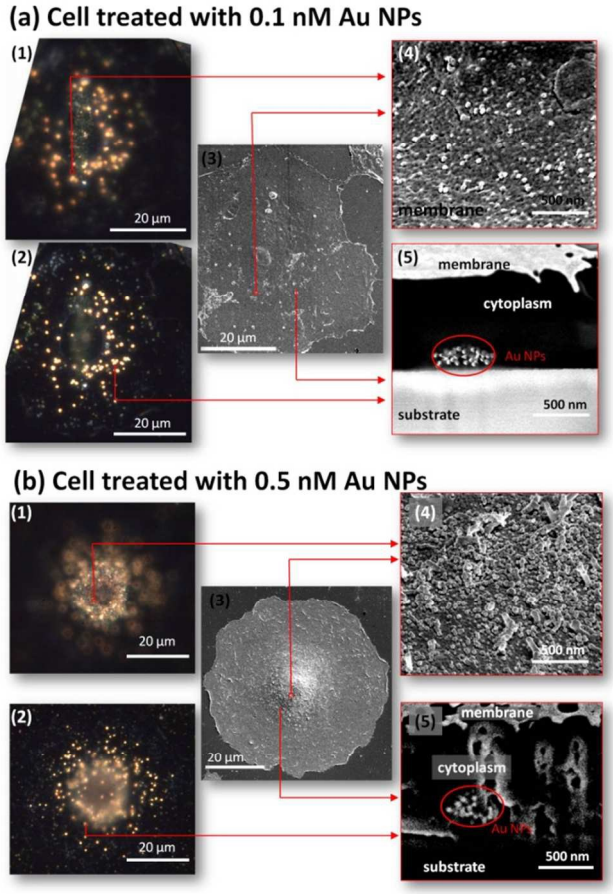

Fig. 6 Scattering images of cells treated with (a) 0.1 and (b) 0.2 nM of Au NPs at (1) z = 0.96 and (2) z = 4.8 μm. As well as (3) their corresponding SEM images, (4) 52° tilted and (5) sectional SEM images cut by DBFIB. Note, because there are a 15 degree rotation in the scattering images in (a), to have a better comparison with SEM images, the scattering images from the dark field microscope was rotated and cropped

Dose dependent cytotoxicity test

The cytotoxicity with different treated dose was examined by using MTT assay. Fig. 7(a) shows the result. With the increase in treated dose, the cellular viability was decreased. We attribute the cytotoxicity is partly from the increase of the Au NPs clusters inside the cells, especially in the lysosomes. In previous studies, a number of evidences indicate that the cytotoxicity of metal NPs is majorly from the release of the toxic ions, such as Ag^{+}, $Au^{1+/3+}$, Cd^{2+} ions, in the acidic environment of lysosomes.[22, 40-42] From scattering images in Fig. 2, we can find that with the increasing of the treated dose, the number of Au NPs cluster inside cell is also increasing, and thus, the result is also consistent with previous efforts.[43]

Furthermore, in most efforts, the toxicity is regarded as the

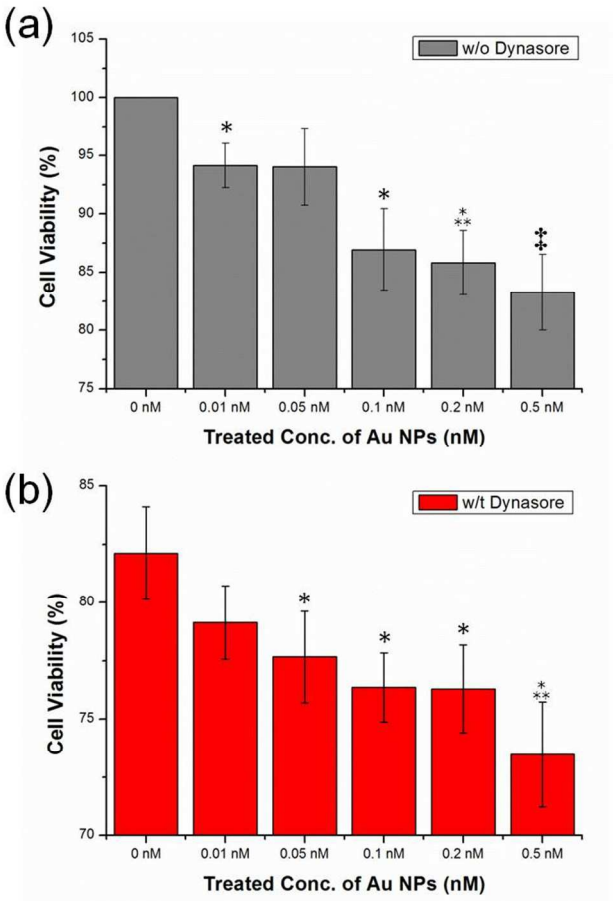

Fig.7 Cell viability with different treated dose of Au NPs (a) without and (b) with 160 μM dynasore treating. * p-value < 0.05, ‡ p-value < 0.01, ** p-value <0.005. Data comes from 5 independent experiments.

"Trojan horse effect" as major.[42, 44, 45] However, in this work, we find Au NPs would not only be stuck inside cells, but also stacked on the membrane. To evaluate whether the stacked Au NPs on membrane would additionally impact the cell viability or not, a controlled experiment, cells treated with different doses of Au NPs while pre-treated with dynasore, was performed. Fig. 7(b) shows the result. Under the inhibition of receptor-mediated endocytosis caused by dynasore, all Au NPs are assumed stuck on the membrane. From the result, although the inhibition of endocytosis would affect the cell viability, a series of Au NPs' treatment on the membrane additionally impacts the cell viability. Different from the acidic environment in lysosomes, the membrane should be a relative neutral environment. It means that there should be no release of the toxic ions, $Au^{1+/3+}$. Therefore, we think it might be due to the physical influence, the pressure from the Au NPs on the membrane. With the increase of the loading on the membrane, Au NPs would hugely influence the cell metabolism.

Some studies have pointed out that both of chemical and physical reason would induce different kinds of cellular responses, such as apoptosis, proliferation, and migration.[46-48] However, there is still no exact explanation for the influence. In this work, we verify that the interaction between NPs and cells is not only inside cells, but also nu-endocytosed NPs on membrane would affect the cellular behaviour. Both of them should be considered as same important factor in the NPs-cells studies.

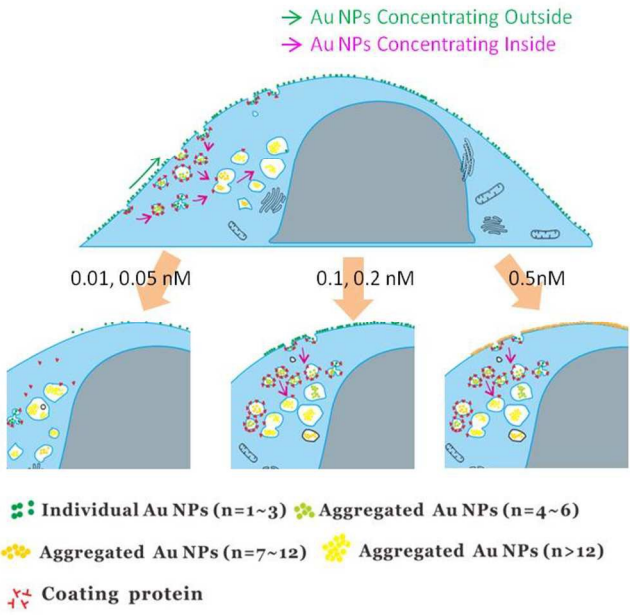

Fig.8 Illustration for different evolution of cellular uptake with different treated dose of Au NPS.

Conclusions

In summary, we show different evolutions of Au NPs uptake with different treated doses by using the dark field microscopy and SEM. In the lower treated doses, 0.01 and 0.05 nM, most NPs can be endocytosed smoothly and clustered inside endocytic vesicles with a larger aggregated number. While with the higher treated doses, 0.1 and 0.2nM, the traffic jam of the endocytosis was occurred. Although the clusters inside cells increased, lots of Au NPs started to be stuck on the membrane. Accompanied by the periodic lamellipodial contraction with rearward actin polymerization on the membrane, stuck Au NPs were then moved to the top of cells. It results two distinct scatter color band, yellow in cells and green on membrane. Furthermore, when the number of stuck Au NPs was too larger, the highest treated dose-0.5 nM in this work, stuck Au NPs were further started to aggregate on the top of cells. Two bands with same scatter color were then shown. SEM images further validated the different aggregations of Au NPs on the membrane. Higher treated dose results in the higher density of Au NPs. DBFIB and tilted SEM images indicated different aggregated situation of Au NPs inside cells and on membrane, 3D stacking and 2D covering respectively. Fig. 8 illustrates the different aggregated situation with different treated dose of Au NPs. MTT analysis also revealed the influence of Au NPs with the different treated dose. Generally, higher treated dose induces higher cytotoxicity. However, the dynasore pre-treated cytotoxicity test further prove the higher cytotoxicity of higher treated dose did not only come from the Au NPs inside cells, but also from the stuck NPs on the membrane. High concentration Au NPs could increase the total number of cellular uptake, but might lower the yield of Au NP's entry due to a traffic jam at the entrance of endocytosis and even increase the side-effect of the use of Au NPs as contrast agents or drug/gene

carrier. In previous studies, major works focus on the endocytosed or penetrated Au NPs inside cells. The influence from Au NPs stuck on the membrane is often limited. This work highlights the importance of an overall distribution of Au NPs in the NPs-cell interacted system.

Acknowledgements

The authors thank Dr. Chau-Hwang Lee and Miss Huei-Jyuan Pan for assistance with cell culture. The tilted and sectional SEM image was supported by DBFIB core facility in Research Center for Applied Sciences, Academia Sinica. This work was supported by the Ministry of Science and Technology of Taiwan, under Project MOST 103-2221-E-001-013-MY3. Technical support from the core facilities for nanoscience and nanotechnology, Academia Sinica in Taiwan, is acknowledged.

Notes and references

[a] Department of Engineering and System Science, National Tsing-Hua University, No.101, Sec. 2, Kuang-Fu Road, Hsinchu, Taiwan 30013, R.O.C.
[b] Research Center for Applied Sciences, Academia Sinica, Taipei 11529, Taiwan. *E-mail: pkwei@gate.sinica.edu.tw; Fax: +886-2-2787-3146; Tel: +886-2-2787-3122*
[c] Institute of Biophotonics, National Yang-Ming University, No.155, Sec.2, Linong Street, Taipei, Taiwan 11221, R.O.C.

‡ These authors contributed equally to this work.

1. C. W. Lee, M. J. Chen, J. Y. Cheng and P. K. Wei, *J. Biomed. Opt.*, 2009, **14**, 034016.
2. S. Patskovsky, E. Bergeron, D. Rioux and M. Meunier, *Journal of biophotonics*, 2014, **5**, 401-407.
3. F. Wang, Y.-C. Wang, S. Dou, M.-H. Xiong, T.-M. Sun and J. Wang, *Acs Nano*, 2011, **5**, 3679-3692.
4. L. Xu, Y. Liu, Z. Chen, W. Li, Y. Liu, L. Wang, Y. Liu, X. Wu, Y. Ji, Y. Zhao, L. Ma, Y. Shao and C. Chen, *Nano Lett.*, 2012, **12**, 2003-2012.
5. I. H. El-Sayed, X. Huang and M. A. El-Sayed, *Cancer Letters*, 2006, **239**, 129-135.
6. W. Jiang, B. Y. S. Kim, J. T. Rutka and W. C. W. Chan, *Nature Nanotechnology*, 2008, **3**, 145-150.
7. J. M. de la Fuente, C. C. Berry, M. O. Riehle and A. S. G. Curtis, *Langmuir*, 2006, **22**, 3286-3293.
8. A. Verma, O. Uzun, Y. Hu, Y. Hu, H.-S. Han, N. Watson, S. Chen, D. J. Irvine and F. Stellacci, *Nature Materials*, 2008, **7**, 588-595.
9. K. Unfried, C. Albrecht, L.-O. Klotz, A. V. Mikecz, S. Grether-Beck and R. P. F. Schins, *Nanotoxicology*, 2007, **1**, 52-71.
10. M. L. Etheridge, S. A. Campbell, A. G. Erdman, C. L. Haynes, S. M. Wolf and J. McCullough, *Nanomedicine: Nanotechnology, Biology and Medicine*, 2013, **9**, 1-14.
11. A. Shapira, Y. D. Livney, H. J. Broxterman and Y. G. Assaraf, *Drug resistance updates*, 2014, **14**, 150-163.
12. N. Lewinski, V. Colvin and R. Drezek, *Small*, 2008, **4**, 26-49.
13. P. V. AshaRani, G. Low Kah Mun, M. P. Hande and S. Valiyaveettil, *Acs Nano*, 2008, **3**, 279-290.
14. N. Chen, Y. He, Y. Su, X. Li, Q. Huang, H. Wang, X. Zhang, R. Tai and C. Fan, *Biomaterials*, 2012, **33**, 1238-1244.
15. Y. Pan, S. Neuss, A. Leifert, M. Fischler, F. Wen, U. Simon, G. Schmid, W. Brandau and W. Jahnen-Dechent, *Small*, 2007, **3**, 1941-1949.
16. C. M. Goodman, C. D. McCusker, T. Yilmaz and V. M. Rotello, *Bioconjugate Chem.*, 2004, **15**, 897-900.
17. N. Pernodet, X. Fang, Y. Sun, A. Bakhtina, A. Ramakrishnan, J. Sokolov, A. Ulman and M. Rafailovich, *Small*, 2006, **2**, 766-773.
18. T. Mironava, M. Hadjiargyrou, M. Simon, V. Jurukovski and M. H. Rafailovich, *Nanotoxicology*, 2010, **4**, 120-137.
19. J. Davda and V. Labhasetwar, *International Journal of Pharmaceutics*, 2002, **233**, 51-59.
20. L. Wang, Y. Liu, W. Li, X. Jiang, Y. Ji, X. Wu, L. Xu, Y. Qiu, K. Zhao, T. Wei, Y. Li, Y. Zhao and C. Chen, *Nano Lett.*, 2011, **11**, 772-780.
21. N. M. Schaeublin, L. K. Braydich-Stolle, A. M. Schrand, J. M. Miller, J. Hutchison, J. J. Schlager and S. M. Hussain, *Nanoscale*, 2011, **3**, 410-420.
22. S. Sabella, R. P. Carney, V. Brunetti, M. A. Malvindi, N. Al-Juffali, G. Vecchio, S. M. Janes, O. M. Bakr, R. Cingolani and F. Stellacci, *Nanoscale*, 2014, **6**, 7052-7061.
23. X. Ma, Y. Wu, S. Jin, Y. Tian, X. Zhang, Y. Zhao, L. Yu and X.-J. Liang, *Acs Nano*, 2011, **5**, 8629-8639.
24. R. Tedja, M. Lim, R. Amal and C. Marquis, *Acs Nano*, 2012, **6**, 4083-4093.
25. A. Albanese and W. C. W. Chan, *Acs Nano*, 2011, **5**, 5478-5489.
26. A. E. Nel, L. Mädler, D. Velegol, T. Xia, E. M. V. Hoek, P. Somasundaran, F. Klaessig, V. Castranova and M. Thompson, *Nature Materials*, 2009, **8**, 543-557.
27. L. O. Herrmann, V. K. Valev, J. Aizpurua and J. J. Baumberg, *Opt. Express*, 2013, **21**, 32377-32385.
28. S. H. Wang, C. W. Lee, M. Y. Pan, S. Y. Hsieh, F. G. Tseng and P. K. Wei, *Plasmonics*, 2015, **10**, 873-880.
29. E. C. Cho, J. W. Xie, P. A. Wurm and Y. N. Xia, *Nano Lett.*, 2009, **9**, 1080-1084.
30. J. Aaron, K. Travis, N. Harrison and K. Sokolov, *Nano Lett.*, 2009, **9**, 3612-3618.
31. J. Panyam and V. Labhasetwar, *Pharmaceutical Research*, 2003, **20**, 212-220.
32. B. D. Chithrani and W. C. W. Chan, *Nano Lett.*, 2007, **7**, 1542-1550.
33. S. H. Wang, C. W. Lee, F. G. Tseng, K. K. Liang and P. K. Wei, *Journal of biophotonics*, 2015.
34. E. Macia, M. Ehrlich, R. Massol, E. Boucrot, C. Brunner and T. Kirchhausen, *Developmental Cell*, 2006, **10**, 839-850.
35. T. Kirchhausen, E. Macia, H. E. Pelish, C. J. D. William E. Balch and H. Alan, in *Methods in Enzymology*, Academic Press, 2008, vol. Volume 438, pp. 77-93.
36. L. Foret, J. E. Dawson, R. Villaseñor, C. Collinet, A. Deutsch, L. Brusch, M. Zerial, Y. Kalaidzidis and F. Jülicher, *Current Biology*, 2012, **22**, 1381-1390.
37. B. D. Chithrani, *Molecular Membrane Biology*, 2010, **27**, 299-311.
38. G. Giannone, B. J. Dubin-Thaler, H.-G. Döbereiner, N. Kieffer, A. R. Bresnick and M. P. Sheetz, *Cell*, 2004, **116**, 431-443.
39. B. Qualmann, M. M. Kessels and R. B. Kelly, *The Journal of cell biology*, 2000, **150**, F111-F116.
40. T.-G. Iversen, T. Skotland and K. Sandvig, *Nano Today*, 2011, **6**, 176-185.

41. S. J. Soenen, P. Rivera-Gil, J.-M. Montenegro, W. J. Parak, S. C. De Smedt and K. Braeckmans, *Nano Today*, 2011, **6**, 446-465.
42. E.-J. Park, J. Yi, Y. Kim, K. Choi and K. Park, *Toxicology in Vitro*, 2010, **24**, 872-878.
43. A. M. Alkilany, P. K. Nagaria, C. R. Hexel, T. J. Shaw, C. J. Murphy and M. D. Wyatt, *Small*, 2009, **5**, 701-708.
44. R. F. Service, *Science*, 2010, **330**, 314.
45. J. F. Kukowska-Latallo, K. A. Candido, Z. Cao, S. S. Nigavekar, I. J. Majoros, T. P. Thomas, L. P. Balogh, M. K. Khan and J. R. Baker, *Cancer research*, 2005, **65**, 5317-5324.
46. E. M. Redmond, P. A. Cahill, M. Hirsch, Y.-N. Wang, J. V. Sitzmann and S. S. Okada, *Thromb Haemost*, 1999, **81**, 293-300.
47. D. D. Nalayanda, W. B. Fulton, P. M. Colombani, T.-H. Wang and F. Abdullah, *Journal of pediatric surgery*, 2014, **49**, 61-65.
48. N. J. Douville, P. Zamankhan, Y.-C. Tung, R. Li, B. L. Vaughan, C.-F. Tai, J. White, P. J. Christensen, J. B. Grotberg and S. Takayama, *Lab on a chip*, 2010, **11**, 609-619.